Progress In Electromagnetics Research M, Vol. 98, 89–99, 2020

A Novel Radar Waveform Design for Anti-Interrupted Sampling Repeater Jamming via Time-Frequency Random Coded Method

Ji Li[1], Xiang Luo[1], Xingyan Duan[1], Wei Wang[1, *], and Jianping Ou[2, *]

Abstract—According to the orthogonality of each sub-carrier in the multi-carrier phase-coded (MCPC) signal, this paper focuses on anti-interrupted sampling repeater jamming (ISRJ) and creatively proposes a novel radar signal based on time-frequency random coded (TFRC) method, namely TFRC-MCPC signal. Based on the perspective of waveform design, the TFRC-MCPC signal adopts a chaotic sequence with good pseudo-random to code each chip in time-domain and each subcarrier in frequency-domain. The TFRC method increases the pseudo-randomness of radar waveform pulses and reduces the correlation between radar echo and ISRJ, thereby effectively suppressing the interference of false targets. The TFRC-MCPC method and common filter design methods do not conflict with each other and can be used in combination. The simulation experiment results show that under the typical parameters described in the paper, compared with the traditional MCPC signal and LFM signal, the signal-jamming ratio (SJR) improvement factor of the TFRC-MCPC signal is optimized by 1–2 dB after pulse compression, which verifies its feasibility and effectiveness.

1. INTRODUCTION

With the rapid development of electronic warfare technology in recent years, considerable attention has been paid to the electromagnetic jamming and anti-jamming for radar system in the electronic countermeasure (ECM) community. To complicate or prevent the radar target detection and recognition, much work has been done on the jamming and anti-jamming techniques.

As a classic jamming type derived from digital radio frequency memory (DRFM) [1–3], the ISRJ is more likely to generate multiple false targets after pulse compression because of its strong correlation with radar signals. The new ISRJ patterns include frequency shift modulation [4], smart noise modulation [5], interrupted sampling signal modulation [6–8], etc. However, compared with interference technology, the research of anti-ISRJ interference technology [9] is relatively insufficient, most of which are aimed at radar echo signals, and anti-jamming processing is performed in the signal processing stage, such as filter design methods.

Zhou et al. designed an in-pulse orthogonal linear frequency modulation (LFM) phase coded waveform. In view of ISRJ, the waveform was divided into different sub-signals, and its corresponding matched filter was used to reconnoiter, identify and counteract the jamming effectively, but the situation of asynchronous sampling between the jamming and the transmitted signal was not considered [10].

In [9, 11, 12], a filter that can reduce the influence of noise signal and improve the performance of jamming suppression under the condition of low signal-to-noise ratio (SNR) was designed by using time-frequency analysis characteristics. In [13, 14], two improved bandpass filter interference suppression methods based on energy function through short-time Fourier transform (STFT) were proposed. These methods have achieved good results in anti-jamming under low SNR. However, the minimum value of

Received 23 July 2020, Accepted 26 October 2020, Scheduled 6 November 2020

* Corresponding author: Wei Wang (wangwei@csust.edu.cn), Jianping Ou (ojpojp133@126.com).

[1] School of Computer and Communication Engineering, Changsha University of Science & Technology, Changsha 410114, China.

[2] ATR key Lab., National University of Defense Technology, Changsha 410073, China.

the energy function needs to be calculated in time and frequency domains, respectively, which results in more complicated calculations.

An energy function detection and band-pass filtering (EFDBP) method was proposed in [15], which constructed the energy function and extracted the undisturbed signal segments by setting a detection threshold. This method was simple, but the effect of jamming suppression was unstable at low SNR and SJR situations.

In [16], the parameters of the waveform were real-time adjusted by the orthogonal coding and waveform diversity in the adaptive pulse, so that the jamming signal and target signal were orthogonal in the radar receiver. This method attempted to suppress the jamming from the perspective of the transmitting system, making it possible to completely separate the jamming from the echo signal. However, the jamming suppression performance is degraded due to the reduction of the transmitting power of the jamming, so it is usually applied to the case where the jamming delay is one or more pulse repetition cycles.

The idea of reconstruction and elimination method was proposed in [17, 18]. This method estimated both the ISRJ parameters (such as the number of intercepted slices and forwarding times) by analyzing the time-frequency results after pulse compression and the slice width by deconvolution. Then the jamming signal was reconstructed according to the estimated parameters. At last, the jamming was suppressed by iteration cancellation.

An in-pulse stepping LFM waveform was designed in [19]. By using the idea of sub-pulse shielding and orthogonality, the jamming and target were sorted by bandpass filter bank and sub-pulse matched filter bank. Therefore, the jamming can be eliminated according to the jamming suppression threshold.

According to the analysis of the above methods, this paper proposes an anti-ISRJ method based on TFRC method and MCPC signal, namely TFRC-MCPC signal, from the perspective of waveform design.

The orthogonal frequency-division multiplexing (OFDM) based MCPC radar signal is obtained by the OFDM based multi-carrier technology and phase encoding. It achieves more balanced effects in three aspects: the main-to-sidelobe ratio in the ambiguity function, envelope fluctuation control, and spectrum utilization. Moreover, due to the flexibility and unpredictability of subcarrier and phase coding patterns, the MCPC-OFDM signal has a strong anti-jamming performance [20, 21].

The TFRC method introduces a new concept of carrier random coding, and chaotic binary codes are used to code each chip in time-domain and each carrier in frequency-domain to achieve the goal of improving the anti-jamming performance in the waveform generation stage.

2. PRINCIPLE OF ISRJ

ISRJ is a brand-new coherent jamming method of broadband radar based on DRFM. By using DRFM to process the radar signal with low-rate interrupted sampling, the interrupted "under-sampling" technology is used to produce the jamming effect of coherent false target beams.

As a periodic sampling from radar signal, sampling and forwarding are executed alternately in the interrupted sampling process. Because the jamming is sampled from the original radar signal, it has greater coherence and can obtain the pulse compression gain. According to the different forms of jamming, ISRJ can be divided into interrupted sampling direct repeater jamming (ISDRJ) and interrupted sampling repetitive repeater jamming (ISRRJ). Different forwarding modes can cause different interference effects. ISDRJ executes sampling once in every sampling period and forwarding it directly after each sampling period. ISRRJ repeats the sampled signal throughout the interval until the next sampling begins, as shown in Fig. 1.

The interrupted sampling function of DRFM-based repeater jammer can be described as [22, 23]:

$$p(t) = \mathrm{rect}\left(\frac{t}{\tau}\right) \otimes \sum_{n=-\infty}^{+\infty} \delta(t - nT_s) \tag{1}$$

where τ is the sampling duration; $\mathrm{rect}(t/\tau)$ is a rectangle envelope pulse with the value $1\,(0 \le t \le \tau)$ or $1\,(otherwise)$; $\otimes$ represents the convolution operation; T_s is the pulse repeat interval; and $D_r = \tau/T_s$ denotes the sampling duty cycle.

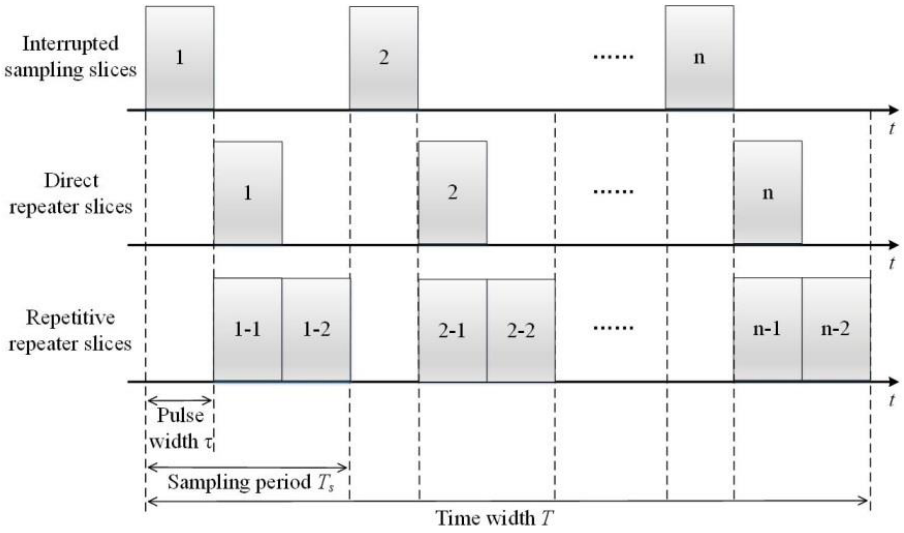

Figure 1. Schematic diagram of the two types of ISRJ.

3. SIGNAL MODEL

Different from the filter design approaches which are most popularly used currently, TFRC-MCPC, carried on the perspective of waveform design, adopts chaotic sequences with good pseudo-randomness to code each chip in time-domain and each carrier in frequency-domain, respectively. Therefore, there is a certain degree of de-correlation between pulses and intra-pulse carriers, thus forming the pseudo-randomness of radar signals. For the new radar signal design in this paper, ISRJ cannot obtain the time-frequency characteristics of the entire pulse, thereby effectively reducing the correlation between the jamming signal and the radar echo signal, and achieving the purpose of anti-jamming [24, 25].

The TFRC-MCPC signal has the following characteristics:

(1) The signal of TFRC-MCPC is composed of P subcarriers, each of which contains M bits of phase coding, and each chip of phase coding has the same width.

(2) To ensure the orthogonality between subcarriers, the frequency intervals between adjacent subcarriers are reciprocal of the chip width. The TFRC-MCPC signal provides a more flexible framework of waveform design.

(3) Different modulation modes can be used in time-domain. The amplitudes and phases of the subcarriers can be weighted in frequency-domain.

The MCPC signal has a good performance of low interception and anti-jamming. Then, the complex envelope $x(t)$ of TFRC-MCPC signal can be expressed as:

$$x(t) = \sum_{p=1}^{P} \omega_p u_p(t) \exp(j2\pi f_p t) = \sum_{p=1}^{P} \sum_{m=1}^{M} \omega_p \varepsilon_{p,m} \eta_p \operatorname{rect}[t - (m-1)t_b] \exp(j2\pi f_p t) \tag{2}$$

where P is the number of carriers; M is the number of coded chips; $\omega_p = |\omega_p| e^{j\phi_p}$, where $|\omega_p|$ is the weighted amplitude on pth subcarrier and ϕ_p the weighted phase; $u_p(t)$ is the complex envelope of subcarrier signal; $f_p = (p-1)(1/t_b)$ is the pth subcarrier frequency; t_b is the time duration of a single chip; $\Delta f = 1/t_b$ represents the subcarrier frequency interval; η_p is the carrier coding of the pth subcarrier; and $\varepsilon_{p,m}$ is the phase coding of the mth chip on the pth subcarrier. The echo signal of the scattering target at the distance R is:

$$x_r(t) = Ax(t - \Delta t) = A \sum_{p=1}^{P} \sum_{m=1}^{M} \omega_p \varepsilon_{p,m} \times \eta_p \operatorname{rect}[t - \Delta t - (m-1)t_b] \exp[j2\pi f_p (t - \Delta t)] \tag{3}$$

where A is the echo amplitude, $\Delta t = 2R/c$ the time delay, and c the speed of propagation. To form coherent false targets jamming, the ISRJ method samples and stores radar signals received by jammers intermittently, and then transmits them after frequency and amplitude modulation. Assuming that the relative distance between jammer and radar is R_j, the interrupted sampling jamming signal can be described as:

$$x_j(t) = \sum_{n=0}^{N_S} \sum_{p=1}^{P} \sum_{m=1}^{M} \omega_p \varepsilon_{p,m} \eta_p \operatorname{rect}\left[\frac{t - \Delta\tau(n)}{\tau}\right] \times \exp\{j2\pi f_p[t - \Delta\tau(n)]\} \tag{4}$$

where $\Delta\tau(n) = t - 2R_j/c - nT_s - t_0$, t_0 is the signal processing delay of the jammer, n the repeat times, N_s the upper limit of forwarding times, and $n(t)$ the Gaussian noise. The total received echo can be described as [26, 27]:

$$x_{\text{echo}}(t) = x_r(t) + x_j(t) + n(t) \tag{5}$$

The time-frequency structure of the TFRC-MCPC signal is shown in Fig. 2.

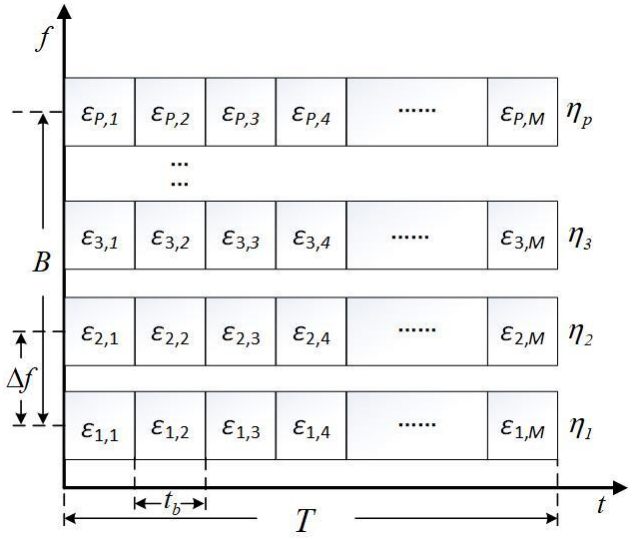

Figure 2. Time-frequency structure of the TFRC-MCPC signal.

$B = P * \Delta f$ is the signal bandwidth, and $T = M * t_b$ is the signal time-duration. Compared with the OFDM signal, the TFRC-MCPC signal has one more modulation dimension, which makes the modulation mode of the signal more flexible. In Fig. 2, each subcarrier can be coded randomly.

To analyze the anti-jamming effect of the TFRC-MCPC signal, the ambiguity function can be calculated as follows.

$$\begin{aligned}
\chi(\tau, v) &= \int_{-\infty}^{\infty} x(t)x^*(t+\tau)\exp(j2\pi vt)dt \\
&= \sum_{p=1}^{P}\sum_{l=1}^{P} \omega_p\omega_l^*\eta_p\eta_l^* \int_{-\infty}^{\infty} u_p(t)u_l^*(t+\tau)\exp(j2\pi f_p t) \times \exp[-j2\pi f_l(t+\tau)]\exp(j2\pi vt)dt \\
&= \sum_{p=1}^{P}\sum_{l=1}^{P} \omega_p\omega_l^*\eta_p\eta_l^*\exp(-j2\pi l\Delta f\tau) \int_{-\infty}^{\infty} u_p(t)u_l^*(t+\tau)\exp\{[j2\pi(p-l)\Delta ft + j2\pi vt]\}dt \\
&= \sum_{p=1}^{P} \omega_p^2\eta_p^2\exp(-j2\pi p\Delta f\tau) \sum_{q=-M}^{M} \chi_u(\tau - qt_b, v)
\end{aligned}$$

$$\sum_{m=1}^{M-|q|} \varepsilon_{p,m}\varepsilon_{p,m+q}^{*} \exp(j2\pi vmt_b) + \sum_{p=1}^{P}\sum_{l=1,p\neq l}^{P} \omega_p\omega_l^{*}\eta_p\eta_l^{*}$$

$$\times \exp(-j2\pi l\Delta f\tau) \sum_{q=i}^{i+1} \chi_u[\tau - qt_b, (p-l)\Delta f + v] \cdot \sum_{m=1}^{M} \varepsilon_{p,m}\varepsilon_{l,m+q}^{*} \exp(j2\pi vmt_b) \quad (6)$$

$$\chi_u(\tau, v) = \begin{cases} \exp[j\pi v(t_b - \tau)] \dfrac{\sin[\pi v(t_b - |\tau|)]}{\pi v(t_b - |\tau|)} \left(1 - \dfrac{|\tau|}{t_b}\right), & |\tau| \leq t_b \\ 0, & |\tau| > t_b \end{cases} \quad (7)$$

where $\chi_u(\tau, v)$ is the ambiguity function of $u(t)$. The ambiguity function of the TFRC-MCPC signal is essentially the result of the frequency shift modulation of $\chi_u(\tau, v)$.

Under the condition of the same time-bandwidth, we simulate the ambiguity function of the TFRC-MCPC signals and compare it with that of LFM signals, as shown in Figures 3–5.

It can be seen from Fig. 3(a) that the TFRC-MCPC signal has the thumbtack-typed ambiguity, and it has a single central peak. Fig. 3(b) shows that the LFM signal has the oblique edged ambiguity.

Comparing the two-dimensional ambiguity figure of the two signals, the resolutions of the two signals in time-domain and frequency-domain are almost the same. The peak values of the mainlobes

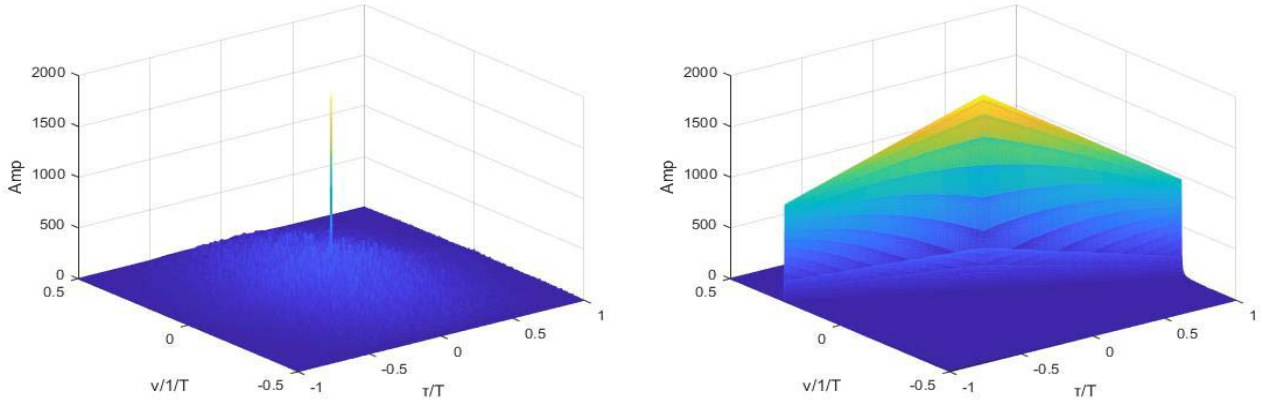

(a) (b)

Figure 3. Three-dimensional ambiguity figure. (a) TFRC-MCPC, (b) LFM.

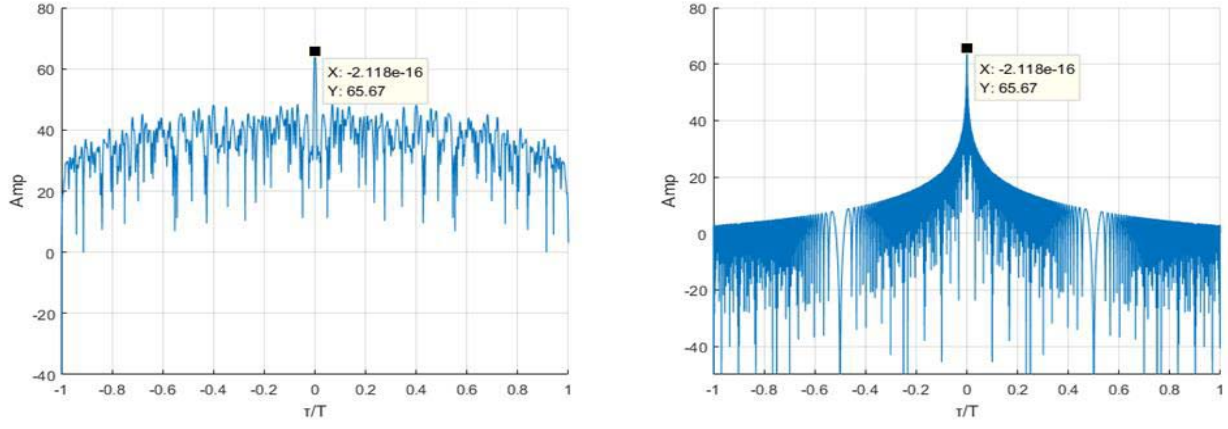

(a) (b)

Figure 4. The cuttings of ambiguity figure on Doppler axis. (a) TFRC-MCPC, (b) LFM.

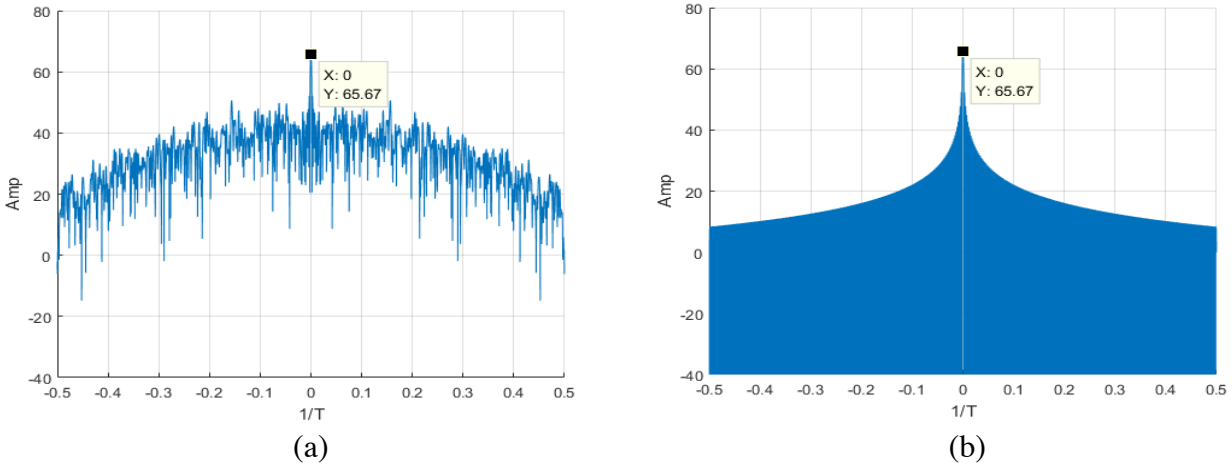

Figure 5. The cuttings of ambiguity figure on time axis. (a) TFRC-MCPC, (b) LFM.

are the same too, and both are 65.67. The mainlobe width of the LFM signal is narrower than that of the TFRC-MCPC signal, so the resolution accuracy of the LFM signal is higher. While the sidelobe peak of LFM is 52.2, and the sidelobe peak of the TFRC-MCPC signal is 47.81, which is smaller than that of the LFM signal, so the resolution of the TFRC-MCPC signal is better than that of the LFM signal. Compared with the oblique edged ambiguity function, the thumbtack-typed ambiguity function has no range-Doppler coupling and lower sidelobe characteristics. Therefore, the TFRC-MCPC signal has a better target detection ability than the LFM signal.

4. JAMMING SUPPRESSION

4.1. Time-Frequency (TF) Characteristics Analysis

TF transform and analysis are commonly applied to analyze TF characteristics of the general signals. However, it is difficult to get certain mathematical expressions of the TF transformation results. For certain signals with only one frequency component all times, the TF characteristics can be denoted explicitly by their instantaneous frequency (IF), which is the derivative of the signal phase. Therefore, we use IF to mathematically analyze the TF characteristics of the target signals and ISRJ signals. According to the analysis of the target echo signal and interference signal in Section 2, the instantaneous frequency of the target echo can be obtained as:

$$\begin{aligned} f_r(t) &= A\sum_{p=1}^{P}\sum_{m=1}^{M}\omega_p\varepsilon_{p,m}\eta_p \times \mathrm{rect}[t-\Delta(t)-(m-1)t_b]\frac{d}{dt}\{f_p[t-\Delta(t)]\} \\ &= A\sum_{p=1}^{P}\sum_{m=1}^{M}\omega_p\varepsilon_{p,m}\eta_p\,\mathrm{rect}[t-\Delta(t)-(m-1)t_b]\cdot f_p \end{aligned} \tag{8}$$

And the IF of ISRJ signal is written as:

$$\begin{aligned} f_j(t) &= A\sum_{n=1}^{N_s}\sum_{p=1}^{P}\sum_{m=1}^{M}\omega_p\varepsilon_{p,m}\eta_p \times \mathrm{rect}\left[\frac{t-\Delta\tau(n)}{\tau}\right]\frac{d}{dt}\{f_p[t-\Delta\tau(n)]\} \\ &= A\sum_{n=0}^{N_s}\sum_{p=1}^{P}\sum_{m=1}^{M}\omega_p\varepsilon_{p,m}\eta_p\,\mathrm{rect}\left[\frac{t-\Delta\tau(n)}{\tau}\right]\times f_p \end{aligned} \tag{9}$$

From Eqs. (8) and (9), it is obvious that the relationship between the frequency and time for ISRJ signal is similar to those of the target signal. Thus, ISRJ can form a group of false targets in pulse

compression results. Based on the discontinuous and periodic characteristics of the ISRJ in the TF domain, we mainly use the STFT result of the radar echo signal to evaluate the matching effect of designed TFRC by calculating the correlation value of corresponding sequences. After calculating the correlation between the discrete frequency-domain waveform and the echo of TFRC, the matching effect of carrier coding can be assessed. We can attain the TF characteristics of radar echo signal $x_r(t)$ by performing STFT, which can be described as [16]:

$$S_{rm}(t,f) = \int_{-\infty}^{\infty} x_r(\tau)\omega(\tau - t)\exp(-j2\pi f\tau)d\tau \tag{10}$$

where $\omega(t)$ is the frequency smoothing window of STFT.

Based on the calculation result of $S_{rm}(t,f)$, the radar echo signal $S(t)$ is obtained by superimposing $|S_{rm}(t,f)|$ in the whole frequency range:

$$S(t) = \sum\nolimits_f |S_{rm}(t,f)| \tag{11}$$

4.2. Suppression Method

In this paper, from the perspective of waveform design, the TFRC-MCPC signal waveform is designed. In 2-dimensional TFRC, the chaotic sequence with good pseudo-randomness is used to code each chip in time-domain and each carrier in frequency-domain, respectively, which increases the pseudo-randomness in radar waveform pulse and reduces the correlation between intermittent sampling interference and radar echo. Therefore, the amplitude of false targets is effectively suppressed [28, 29].

Radar received signal can be obtained by STFT transform:

$$S_m(t,f) = \int_{-\infty}^{\infty} x(\tau)\omega(\tau - t)\exp(-j2\pi f\tau)d\tau \tag{12}$$

The normalized filter can be expressed as:

$$H(f) = |S_m(t,f)|^2 \tag{13}$$

Multiply the designed matched filter function with the total echo signal to obtain the pulse pressure output after the interrupted sampling jamming suppression:

$$P(f) = H(f) \times \int S_m(t)\exp(-j2\pi ft)dt \tag{14}$$

Herein, the SJR improvement factor is adopted to evaluate the jamming suppression performances. It can be represented as

$$\delta_{\mathrm{SJR}} = \mathrm{SJR}_{\mathrm{PC}} - \mathrm{SJR} \tag{15}$$

where $\mathrm{SJR}_{\mathrm{PC}}$ denotes the SJR after pulse compression.

5. SIMULATION ANALYSIS

In order to verify the anti-interference performance of TFRC-MCPC signals, two groups of experiments are designed:

(1) Using TFRC to counter ISRJ;

(2) Assessing the suppression performance.

6. TFRC

In this section, TFRC adopts the chaotic binary phase coded with good pseudo-randomness. Thus, the sampling period is set to an integer multiple of the sampling pulse width. In the experiment, the bandwidth is set to 120 MHz; the pulse width is 4 μs; the number of carriers is 12; the number of chips is 40; the carrier frequency is 30 GHz; the SJR is −3 dB; and the SJR is −6 dB.

The ISDRJ simulation results of the conventional MCPC signal and TFRC-MCPC signal are shown in Fig. 6(a) and Fig. 6(b), respectively. As can be seen in Fig. 6, a single false target that lags the true target is generated in each experiment. In Fig. 6(a), there is a false target with an amplitude of 0.5. However, the amplitude of the false target decreases to 0.315 in Fig. 6(b). In the experiment results of ISDRJ on TFRC-MCPC, both the jamming and harmonic interference band are suppressed obviously.

The ISRRJs of the conventional MCPC signal and TFRC-MCPC signal are shown in Fig. 7(a) and Fig. 7(b), respectively. We can see that ISRRJ can make the MCPC signal produce several realistic false targets, which increases the difficulty of target detection. After using TFRC, the amplitude of the false target signal can be effectively reduced, so the TFRC-MCPC signal can easily suppress the repeater jamming with interrupted sampling.

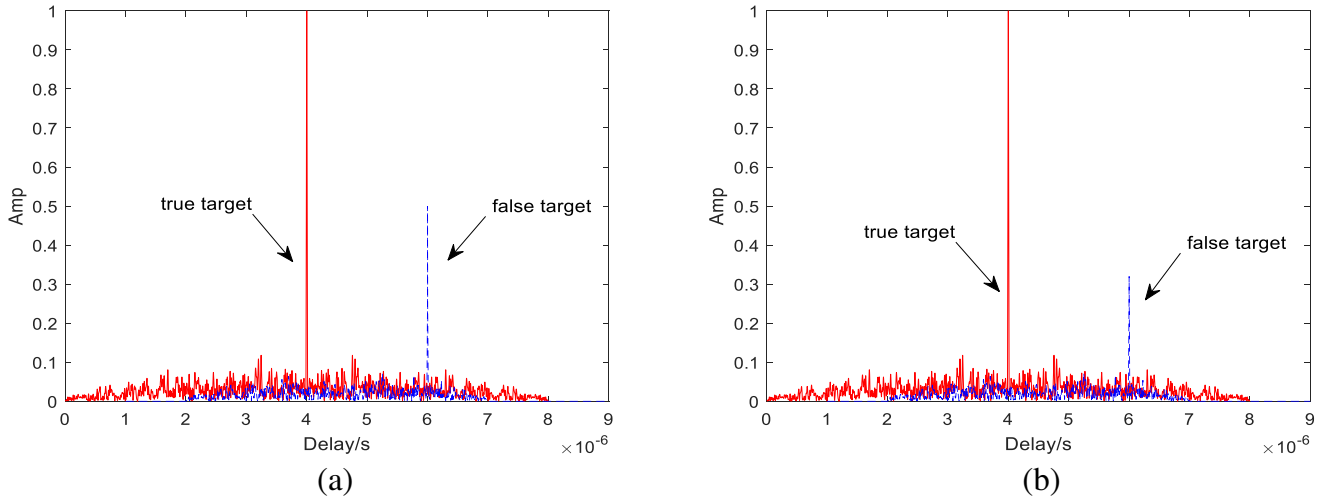

Figure 6. Simulation comparisons of jamming suppression. (a) ISDRJ on MCPC, (b) ISDRJ on TFRC-MCPC.

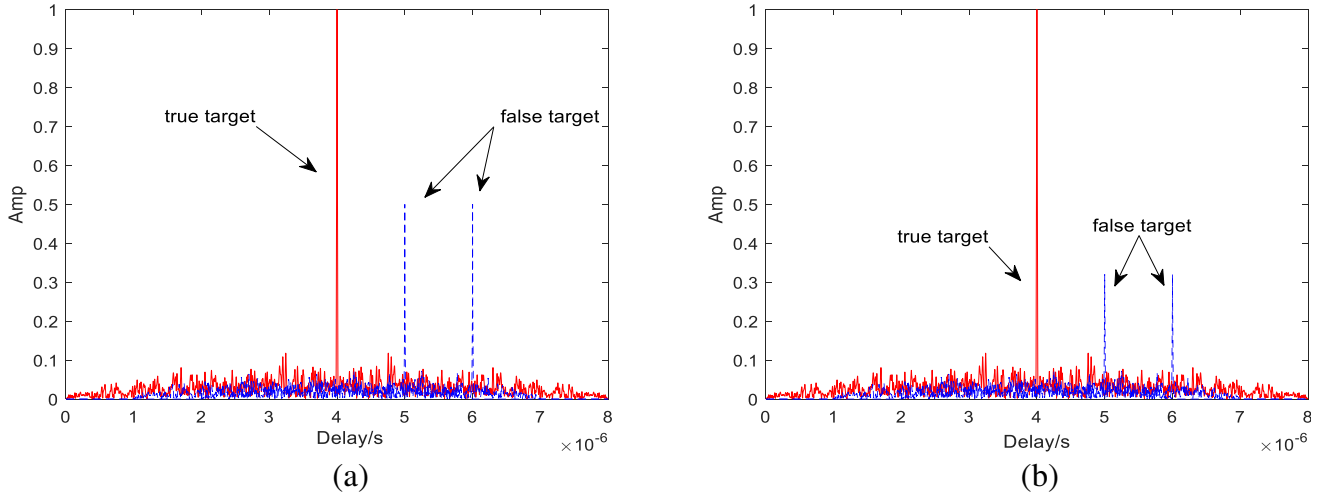

Figure 7. Simulation comparisons of jamming suppression. (a) ISRRJ on MCPC, (b) ISRRJ on TFRC-MCPC.

6.1. Assessing the Suppression Performance

In this part, the interference effects of the three signals of LFM, MCPC, TFRC-MCPC under different SNR and SJR conditions are analysed. The number of Monte Carlo trials is 100 for each of the different SNRs and SJRs. The inputs of the matched filter SJR are −6 dB, −9 dB, −12 dB, and −15 dB. The SJR improvement factor is the output after pulse compression.

As can be seen in Fig. 8, the SJR improvement factor curves of the LFM signal and traditional MCPC signal are not very different. In the TFRC-MCPC signal proposed in this paper, under different SNRs, the SJR improvement factor is higher than that of the LFM signal and MCPC signal, which is about $1 \sim 2$ dB. In addition, the TFRC-MCPC signal is predesigned, which means that it does not require calculations in the signal processing and is easy to implement.

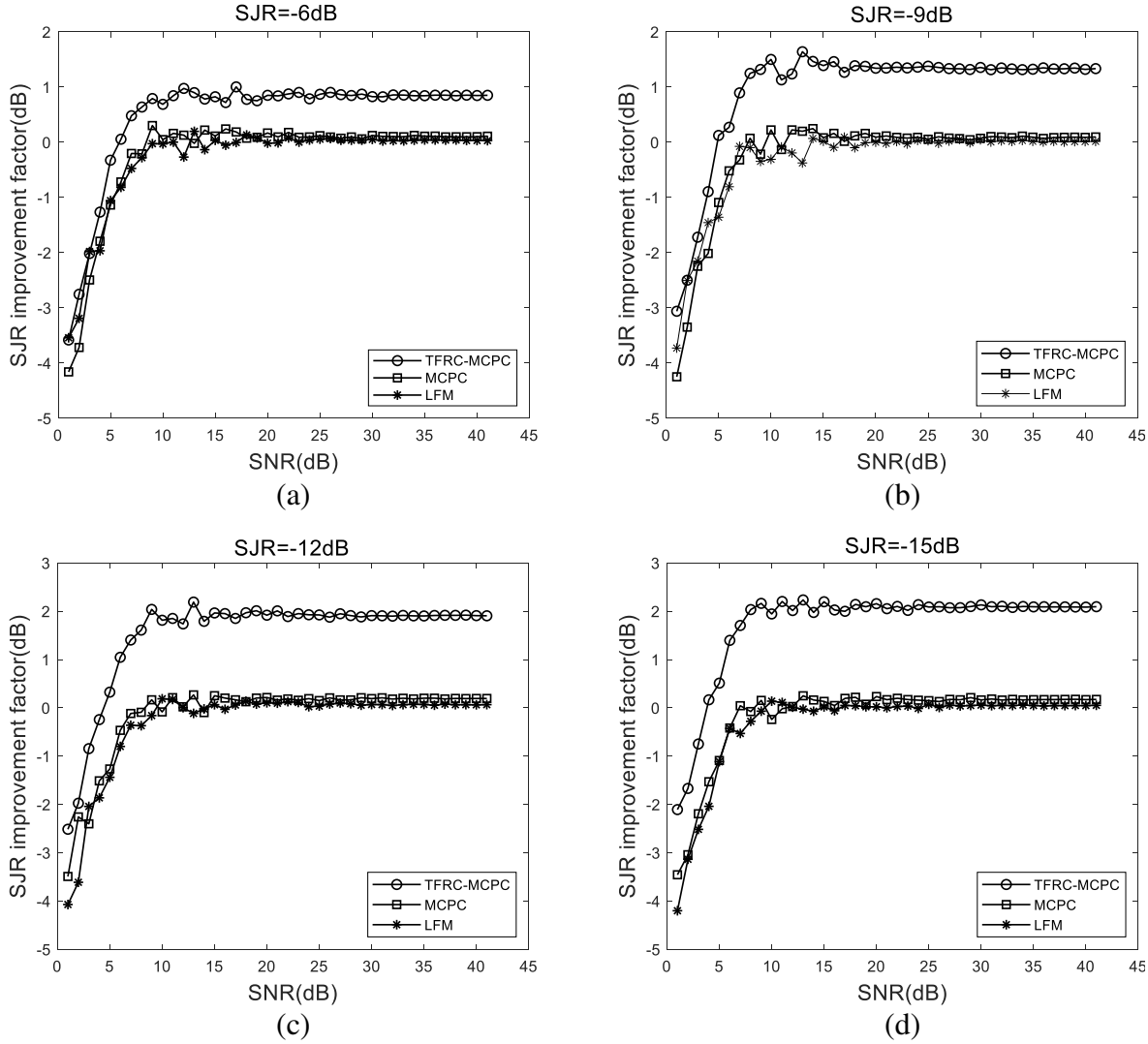

Figure 8. Performances of jamming suppression with different SJRs and SNRs. (a) SJR = −6 dB, (b) SJR = −9 dB, (c) SJR = −12 dB, (d) SJR = −15 dB.

7. CONCLUSION

Increasing attention has been paid to ISRJ, which can greatly complicate the target detection and recognition of wideband radar. Given the discontinuous sampling characteristics on time-domain of ISRJ, this paper proposes a new type of radar signal, TFRC-MCPC signal. The TFRC-MCPC signal

adopts a chaotic sequence with good pseudo-randomness to code each chip in time-domain and each subcarrier in the frequency domain of the traditional MCPC signal. The simulation results verify that the TFRC-MCPC signal can effectively suppress the ISDRJ signals and ISRRJ signals.

The method in this paper does not conflict with existing anti-ISRJ methods, such as matched filter design methods. They can be used in combination to achieve a better suppression effect. This paper introduces a new method in the field of traditional radar to provide a new solution to the radar anti-jamming problem.

In recent years, deep learning method has been widely used in target recognition [30]. Wang et al. studied the recognition of SAR and radar signals by using deep learning method [31, 32]. We can also use the deep learning method to identify the types of radar jamming signals and take corresponding anti-jamming measures in future research.

Funding Statement

This work was supported in part by the National Defense Pre-Research Foundation of China under Grant 7301506, National Natural Science Foundation of China under Grant 61070040, Scientific Research Fund of Hunan Provincial Education Department under Grant 17C0043, and Hunan Provincial Natural Science Fund under Grant2019JJ80105.

REFERENCES

1. Lu, G., S. Liao, S. Luo, and B. Tang, "Cancellation of complicated DRFM range false targets via temporal pulse diversity," *Progress In Electromagnetics Research C*, Vol. 16, 69–84, 2010.
2. Wang, et al., "Mathematic principles of interrupted-sampling repeater jamming (ISRJ)," *Sci. China Ser. F: Inf. Sci.*, Vol. 50, No. 1, 113–123, 2007.
3. Lu, Y. L. and S. Y. Li, "CFAR detection of DRFM deception jamming based on singular spectrum analysis," *Proc. IEEE Int. Conf. Signal Process., Commun. Comput. (ICSPCC)*, 1–6, Xiamen, China, Oct. 2017.
4. Li, C. Z., W. M. Su, and H. Gu, "Improved interrupted sampling repeater jamming based on DRFM," *Proc. IEEE Int. Conf. Signal Process., Commun. Comput. (ICSPCC)*, 254–257, Guilin, Chian, Aug. 2014.
5. Liu, J. B., L. Li, and Z. F. Liu, "Research on smart noise jamming against PD radar," *Inf. Res.*, Vol. 37, 19–21, Feb. 2011.
6. Shen, R., Z. Liu, J. Sui, and X. Wei, "Study on interrupted-sampling repeater jamming performance based on intra-pulse frequency coded signal," *Proc. SPIE*, Vol. 10420, Art. No. 104204, Jul. 2017.
7. Pan, X., W. Wang, D.-J. Feng, J. Huang, Q. Fu, and G. Wang, "Rotational micro-motion modulated jamming for countering ISAR based on intermittent sampling repeater," *Progress In Electromagnetics Research C*, Vol. 36, 41–56, 2013.
8. Guo, L., H. Li, and Q. S. Li, "Interrupted sampling smart jamming method for coherent radar," *Mod. Def. Technol.*, Vol. 41, 119–124, Mar. 2013.
9. Wei, X., G. Zhang, and W. Liu, "Efficient filter design against interrupted sampling repeater jamming for wideband radar," *EURASIP J. Adv. Signal Process.*, Vol. 9, 1–12, Dec. 2017.
10. Zhou, C., Z. Y. Tang, and F. L. Yu, "Anti intermittent sampling repeater jamming method based on intrapulse orthogonality," *J. Syst. Eng. Electron.*, Vol. 2, 269–275, 2017.
11. Gong, S. X., X. Z. Wei, and X. Li, "ECCM scheme against interrupted sampling repeater jammer based on time-frequency analysis," *J. Syst. Eng. Electron.*, Vol. 25, No. 6, 996–1003, Dec. 2014.
12. Zhou, C., F. F. Liu, and Q. H. Liu, "An adaptive transmitting scheme for interrupted sampling repeater jamming suppression," *Sensors*, Vol. 17, No. 11, 2480, 2017, doi: 10.3390/s17112480.
13. Aubry, A., A. D. Maio, and Y. W. Huang, "Robust design of radar Doppler filters," *IEEE Trans. Signal Process.*, Vol. 64, No. 22, 5848–5860, Nov. 2016.
14. Yuan, H., C. Y. Wang, and L. An, "ECCM scheme against interrupted-sampling repeater jamming based on compressed sensing signal reconstruction," *J. Syst. Eng. Electron.*, Vol. 40, No. 4, 717–725, Apr. 2018.

15. Yuan, H., C. Y. Wang, and X. Li, "A method against interrupted-sampling repeater jamming based on energy function detection and band-pass filtering," *Int. Antenn. Propag.*, Vol. 2017, 1–9, Art. No. 6759169, Mar. 2017, doi: 10.1155/2017/6759169.
16. Wei, Z. H., Z. Liu, and P. Bo, "ECCM scheme against interrupted sampling repeater jammer based on parameter-adjusted waveform design," *Sensors*, Vol. 18, No. 4, 1141, 2018.
17. Zhou, C., F. Shi, and Q. Liu, "Research on parameters estimation and suppression for C&I jamming," *Proc. CIE Int. Conf. Radar*, 1–4, Oct. 2016.
18. Zhou, C., Q. Liu, and X. Chen, "Parameter estimation and suppression for DRFM-based interrupted sampling repeater jammer," *IET Radar, Sonar & Navigation*, Vol. 12, No. 1, 56–63, 2018.
19. Zhang, J. Z., H. Q. Mu, S. L. Wen, and Y. B. Li, "Anti intermittent sampling repeater jamming method based on stepped LFM waveform," *Syst. Eng. Electron.*, Vol. 41, 1013–1020, 2019.
20. Huang, Y. L., Y. Zeng, and Y. Fu, "Design and characteristic analysis of multicarrier chaotic phase coded radar pulse train signal," *Int. J. Antenn. Propag.*, Vol. 2014, Art. No. 724294, 2014, doi: 10.1155/2014/724294.
21. Sen, S. and C. W. Glover, "Optimal multicarrier phase-coded waveform design for detection of extended targets," *IEEE Radar Conf.*, 1–4, Ttawa, Canada, Apr. 2013.
22. Yu, M., S. B. Dong, and X. Y. Duan, "A novel interference suppression method for interrupted sampling repeater jamming based on singular spectrum entropy function," *Sensors*, Vol. 19, No. 1, 2019.
23. Chen, J., S. Xu, and J. W. Zou, "Interrupted-sampling repeater jamming suppression based on stacked bidirectional gated recurrent unit network and infinite training," *IEEE Access*, Vol. 7, 107428–107437, Aug. 2019.
24. Davis, R. M., R. L. Fante, and R. P. Perry, "Phase-coded waveforms for radar," *IEEE Trans. Aerosp. Electron. Syst.*, Vol. 43, 401–408, 2007.
25. Tang, L., Y. Zhu, and Q. Fu, "Designing waveform sets with good correlation and stopband properties for MIMO radar via the gradient-based method," *Sensors*, Vol. 17, 999, 2017.
26. Deng, H., "Polyphase code design for orthogonal netted radar systems," *IEEE Trans. Signal Process.*, Vol. 52, 3126–3135, 2004.
27. Yang, Y., R. S. Blum, and Z. S. He, "MIMO radar waveform design via alternating projection," *IEEE Trans. Signal Process.*, Vol. 58, 1440–1445, 2010.
28. Yang, Y. and R. S. Blum, "MIMO radar waveform design based on mutual information and minimummean-square error estimation," *IEEE Trans. Aerosp. Electron. Syst.*, Vol. 43, 330–343, 2007.
29. Chen, Z. K., J. Wang, and X. L. Qiao, "Waveform design for MIMO radar with sparse antenna array," *Proc. 2015 IET Int. Radar Conf.*, 1–5, Hangzhou, China, Oct. 14–16, 2015.
30. Wang, W., Y. Li, T. Zou, X. Wang, J. You, and Y. Luo, "A novel image classification approach via dense-mobile net models," *Mobile Information Systems*, Vol. 2020, Article ID 7602384, 8 pages, 2020.
31. Wang, W., C. Zhang, J. Tian, J. Ou, and I. Li, "A SAR image targets recognition approach via novel SSF-net modelse," *Computational Intelligence and Neuroscienc*, Vol. 2020, Article ID 8859172, 9 pages, 2020.
32. Wang, W., C. Zhang, J. Tian, et al.,"High resolution radar targets recognition via inception-based VGG (IVGG) networks," *Computational Intelligence and Neuroscience*, Vol. 2020, Article ID 8893419, 11 pages, 2020.